KRONOS FUSION ENERGY

PAPER 2.23 · THE KRONOS 2026 SERIES

Cryogenics and the Cold-Mass Thermal Budget of a High-Field Spherical-Tokamak Breeder: Centrepost Heat Loads, Current Leads, and the 4.5 K Refrigeration Plant

The cold-mass thermal budget decides whether a compact spherical tokamak can be built at all, because the toroidal-field current must pass through the tightest radius in the...

Read it live — 3-D model · physics validator · film series

BY P I FORD, R J WEGGEL AND C WEGGEL

2026 · EDITORIAL EDITION

THE OFFICIAL RECORD

What this document is, and how to read its numbers

This is a combined editorial. It gathers, in one volume, the two design studies Kronos Fusion Energy released in 2026 — a compact spherical-tokamak tritium/helium-3 breeder and a deuterium–helium-3 tandem-mirror generator — together with the intellectual-property estate, the people, and, in the internal edition, the full commercial case. The scientific text is the same text that appears in the arXiv preprints and the journal submissions; the editorial adds the apparatus a reader needs to hold the whole program at once, and nothing in the physics is altered to fit it.

THE HONESTY STANCE IS THE ASSET

Every headline quantity carries an **evidence class** — DERIVED RECOMPUTED MEASURED REQUIREMENT — and, where a number is a modelled extrapolation rather than a demonstrated value, it is labelled as such and its downside is shown next to it. Several quantities in the underlying corpus moved after first publication; where a value has been withdrawn or restated, the record says so plainly. This is deliberate: a diligence team will find the load-bearing assumptions, so the document surfaces them first.

TWO EDITIONS

This volume is issued in two editions. The **public edition** (light) carries the physics and the design only — no dollar, price, or per-kilogram figure appears anywhere in it. The **internal edition** (dark) adds the economics, the funding architecture, and the defense-commercial analysis, and is marked *Confidential* accordingly; it is not for public distribution. Where the commercial case rests on a modelled assumption rather than a demonstrated one, it is labelled as such and its downside is shown alongside it, on the same terms as the physics.

TITLE	The Kronos Fleet — Hyperion · Aegis · MetroVolt: A Combined Design & Commercialization Study
AUTHOR	Priyanca Ford, Founder & CEO, on behalf of Kronos Fusion Energy
EDITION	2026 Combined Editorial · first issue
COMPANION WORKS	The five-paper arXiv drop — (1) Breeder, (2) Burner, (3) REBCO magnet & tape, (4) Direct Energy Conversion, (5) AI/ML/Quantum control — with matching numbered Zenodo deposits, plus the IOP journal and IAEA-FEC submissions. Patents were filed before the drop.
NAMING	Hyperion = the breeder; Aegis (defense) and MetroVolt (data-center) = one generator in two housings. Internal mode letters (D1, L) do not appear on public surfaces.
STATUS	Conceptual design & simulation study. Nothing herein is a construction commitment.

HOW TO READ THIS VOLUME

The fleet at a glance, and the way its numbers are marked

This volume opens with *Orientation*, presents the five research papers as a bound sequence, and closes with the *Apparatus*. *Foundations* sets out the three general results both machines rest on. *Paper One* is the Hyperion breeder; *Paper Two* the Aegis / MetroVolt generator; *Papers Three, Four and Five* are the enabling science — high-field REBCO magnets and tape, direct energy conversion, and the AI / ML / quantum control stack. A *Digital Twin & 3-D Model* part follows, then the *Environmental* profile. The *Economics* and levelized cost and the *Business Case* and diligence record appear in the internal edition only; the *Simulations* proof record and the Apparatus — patent portfolio, team, limitations, and sources — close both editions.

THE FLEET AT A GLANCE

	HYPERION	AEGIS	METROVOLT
Role	Strategic-isotope foundry	Defense installation power	Campus power
Machine	**Spherical tokamak**	**Tandem mirror**	**Tandem mirror**
Fuel	Deuterium–tritium	Deuterium–helium-3	Deuterium–helium-3
Delivers	Tritium · ^{3}He · 14 MeV n	Resilient installation power	Firm campus power
Physics bar	**Fusion gain only**	Closure (gates named)	Closure + lunar ^{3}He
In the fleet	Breeds the fuel	Proves the generator	Commercial destination

HOW THE NUMBERS ARE MARKED

Every headline quantity carries an evidence class — DERIVED from first principles, RECOMPUTED from raw data, MEASURED in hardware, or a REQUIREMENT yet to be met. Financial figures carry a case label and are confined to the internal (confidential) edition. Values that moved after first publication are shown as withdrawn or restated rather than quietly changed. A capability you can evaluate is one whose limits are on the page.

ABSTRACT

Cryogenics and the Cold-Mass Thermal Budget of a High-Field Spherical-Tokamak Breeder: Centrepost Heat Loads, Current Leads, and the 4.5 K Refrigeration Plant

The cold-mass thermal budget decides whether a compact spherical tokamak can be built at all, because the toroidal-field current must pass through the tightest radius in the machine, where current density and neutron flux are simultaneously highest. We report the cryogenic case for the Hyperion breeder (design point $I_p = 9.66\,MA$, $Q = 3.076$, $P_{\text{fus}} = 85.04\,MW$, negative triangularity $\delta = -0.30$, $B_0 = 8\,T$, elongation $\kappa = 2.0$, major radius $R_0 = 1.20\,m$, aspect ratio $A = 2.5$, centrepost peak field 16.84 T) and show that high-temperature superconductivity (HTS) is not an optimisation but a requirement. A fully-resistive centrepost would dissipate $\approx 282\,MW - 3.3\times$ the fusion power — which is a non-starter; a fully superconducting REBCO centrepost replaces that dissipation with a cryogenic load of order $\approx 5\,MW$, a reduction of $\approx 56\times$, and a hybrid variant retains only a thin ($\approx 12\,\%$, $\approx 39\,MW$) resistive innermost layer as a radiation-immune sacrificial element. We derive the governing cold-mass heat balance from the conduction, radiation, current-lead, joint, and nuclear-heating channels, and show that the classical parasitic leaks close to well below 0.1 MW at , so the envelope is set by centrepost nuclear heating referred across a staged shield system whose fraction, through the Carnot penalty $(T_h/T_c - 1)/\eta_2 \approx 263\,W/W$, controls the cryoplant wall-plug. The quench transient is made intrinsically safe: a conduction-cooled dry winding removes the helium-expulsion hazard entirely, while a channel-cooled variant is bounded by a $\varnothing 5\,mm$ relief passing 0.44 kg/s that holds a 105 kJ deposit into 0.43 kg of helium to the 20 MPa design pressure. Because normal-zone propagation in REBCO is slow ($\approx 10.5\,cm/s$, $48\times$ below low-temperature superconductor), fast spatial detection is mandatory; a co-wound fibre (52 ms) plus a six-section dump caps the adiabatic hot-spot at 63 K, which in turn holds the combined thermal and electromagnetic von Mises stress to 245 MPa at a safety factor of 3.3 against the 800 MPa allowable. All results were computed on the NVIDIA GPU high-performance-computing campaign and trace to frozen anchors in the Kronos Physics De-Risking Register. The single open item — the centrepost nuclear heating at full three-dimensional fidelity — is bounded by the 5 MW envelope within which the budget already closes.

Open-access deposit (code & data, CC BY 4.0): DOI 10.5281/zenodo.22645840 · Zenodo community *kronos_fusion_energy*. Explore it live: interactive 3-D model · physics validator.

Keywords: cryogenics · cold-mass thermal budget · HTS current leads · REBCO centrepost · refrigeration COP · quench relief · spherical-tokamak breeder

CONTENTS

Table of Contents

NOMENCLATURE

Symbols, units, and the names of things

Q	plasma (fusion) gain, P_{fus}/P_{aux}
Q_E	engineering gain, net electric out / recirculating in
H_{98}	confinement enhancement over the IPB98(y,2) scaling
Z_{eff}	effective ion charge
c_{ee}	electron–electron bremsstrahlung leading coefficient, 2.120022 (exact)
τ_E	energy confinement time
I_p	plasma current
R_0, a	major radius, minor radius
κ, δ	elongation, triangularity
β_N	normalized plasma beta (Troyon-normalized)
TBR	tritium breeding ratio
DEC	direct energy conversion
CF	plant capacity factor (availability)
FOAK / NOAK / BOAK	first / n^{th} / best of a kind
Hyperion	the ST breeder (internal: Mode D2)
Aegis	the generator, defense/installation housing (internal: Mode M)
MetroVolt	the generator, data-center housing (Mode M)

§ 1

Introduction

THE COLD MASS AS THE PACING CONSTRAINT

A superconducting tokamak lives or dies by its cryogenics. Every watt that reaches the cold mass must be removed at a few kelvin, where refrigeration is expensive in wall-plug terms because of the Carnot penalty, and a compact spherical tokamak (ST) makes the problem acute: it forces the toroidal-field (TF) conductors through a narrow centrepost, where the current density and the 14 MeV neutron flux are both maximal. The Hyperion breeder holds $I_p = 9.66\,MA$ at a major radius of only $R_0 = 1.20\,m$ behind a centrepost magnet whose peak field is 16.84 T; the total TF current linking the post is 48 MA and the magnet stores $\approx 1.85\,GJ$ [1]. Whether such a machine is buildable is decided, before any plasma physics, by the answer to a single cryo-engineering question: can the current be carried through that radius without either (i) a dissipation that dwarfs the fusion output, or (ii) a cryogenic load that a refrigeration plant cannot service?

This paper answers that question. We first establish the decisive comparison between a resistive and a superconducting centrepost (§2); we then derive the governing cold-mass heat balance and its component channels—solid conduction, multilayer-insulation radiation, current-lead heat leak, demountable-joint dissipation, nuclear heating, and staged refrigeration—as explicit equations (§3); we describe the NVIDIA GPU high-performance-computing (HPC) campaign and the numerical formulation that produced the results (§4); we present the quantitative results with figures and tables (§5); and we close the quench transient, its relief sizing, and the thermal-stress margin as a coupled cryogenic-structural problem (§5.3, in §5). Every quantitative claim traces to a frozen result in the Kronos Physics De-Risking Register [1]; the serial identifiers (e.g. BR-CX-22, QS-07) are given inline so each number is auditable.

PRIOR ART: HTS FUSION MAGNETS AND THEIR CRYOGENICS

The move to high-temperature superconductor (HTS) rare-earth barium copper oxide (REBCO) tape has been the enabling step for compact, high-field fusion [2,3,4]. REBCO carries very high engineering current density at high field and elevated temperature [5], and cabled conductors such as VIPER [6] and the no-insulation winding technique [7] have taken the concept from tape to magnet, culminating in a 45.5 T all-superconducting DC field [8]. The ARC line of compact high-field tokamaks introduced demountable REBCO magnets to make the vacuum vessel and blanket serviceable, and made the cryogenic and structural consequences of a high-field centrepost a first-order design driver [9]; SPARC has since carried the high-field REBCO pathway toward net energy gain [10]. The cryogenic engineering that underwrites these devices—staged thermal shields, optimised current leads, and quench protection—rests on a mature discipline [11,12,13,14,15] with well-defined scaling laws for conduction, radiation, and refrigeration efficiency [17], and on the large-machine experience of ITER-scale magnet systems [20]. Where a spherical tokamak departs from all of this is in the geometry: the centrepost concentrates field, force, current density and neutron dose into a single slender member, so its cold-mass budget cannot be inherited from a large aspect-ratio machine and must be computed for the ST directly [27].

CONTRIBUTION

This paper contributes (i) the quantitative resistive-versus-HTS argument that fixes the architecture as superconducting; (ii) a formal derivation of the cold-mass heat balance with each channel written as an equation and evaluated at the Hyperion operating point, showing that the parasitic leaks close far below the register envelope and that centrepost nuclear heating referred through a staged shield system sets the load and hence the wall-plug; (iii) a GPU-HPC methodology naming the codes that produced the results and the verification against the frozen register anchors; and (iv) a self-consistent quench-and-relief analysis in which fast, *spatial* detection is shown to be simultaneously the pressure-safety and the structural-margin lever. The result is a cold-mass thermal budget that closes with clear margin and whose single open item is explicitly bounded.

§ 2

The thermal-budget argument: why HTS is required

The centrepost sets the whole cryogenic problem. Consider it first as a resistive conductor. The TF current $I_{\mathrm{TF}} = 48\,MA$ must produce a bore field whose peak is 16.84 T; at the current density this forces through the available annulus, the ohmic dissipation in a normal-metal (copper) post is

$$P_\Omega \;=\; \int_{V_{\mathrm{cp}}} \rho_{\mathrm{Cu}}(T)\, J^2\, \mathrm{d}V \;\approx\; 282\,\mathrm{MW},$$

evaluated with a warm, radiation-degraded copper resistivity over the centrepost volume V_{cp} at the operating current density (BR-CX-22). This is $3.3\times$ the $P_{\mathrm{fus}} = 85.04\,MW$ the machine produces. A reactor that spends more than three times its fusion output pushing current through its own magnet cannot close an energy balance, and this single number—not a marginal efficiency argument—is why the design is superconducting.

A fully superconducting REBCO centrepost removes essentially all of P_Ω: the transport current flows without resistance, and the burden collapses from a *dissipation* of 282 MW to a *refrigeration load* of order $\dot{Q}_{\mathrm{cryo}} \approx 5\,MW$ needed to hold the cold mass at temperature against parasitic and nuclear heat, a reduction of

$$\frac{P_\Omega}{\dot{Q}_{\mathrm{cryo}}} \;\approx\; \frac{282}{5} \;\approx\; 56\times.$$

A hybrid variant deliberately retains a thin resistive innermost layer—about $12\,\%$ of the post, dissipating $\approx 39\,MW$—as a *radiation-immune sacrificial element* in the region of highest neutron damage, with the bulk of the post superconducting; this trades a modest, localised dissipation for tolerance to the fast-neutron fluence that limits REBCO life [1]. In every case the conclusion is identical: HTS is a requirement of the architecture, not a refinement of it (Figure 1, Table 1). It is essential to note that the 5 MW figure is a *cryogenic* load referred across a staged shield system, not 5 MW at ; the distribution of that load across temperature stages, derived below, is what makes the plant tractable.

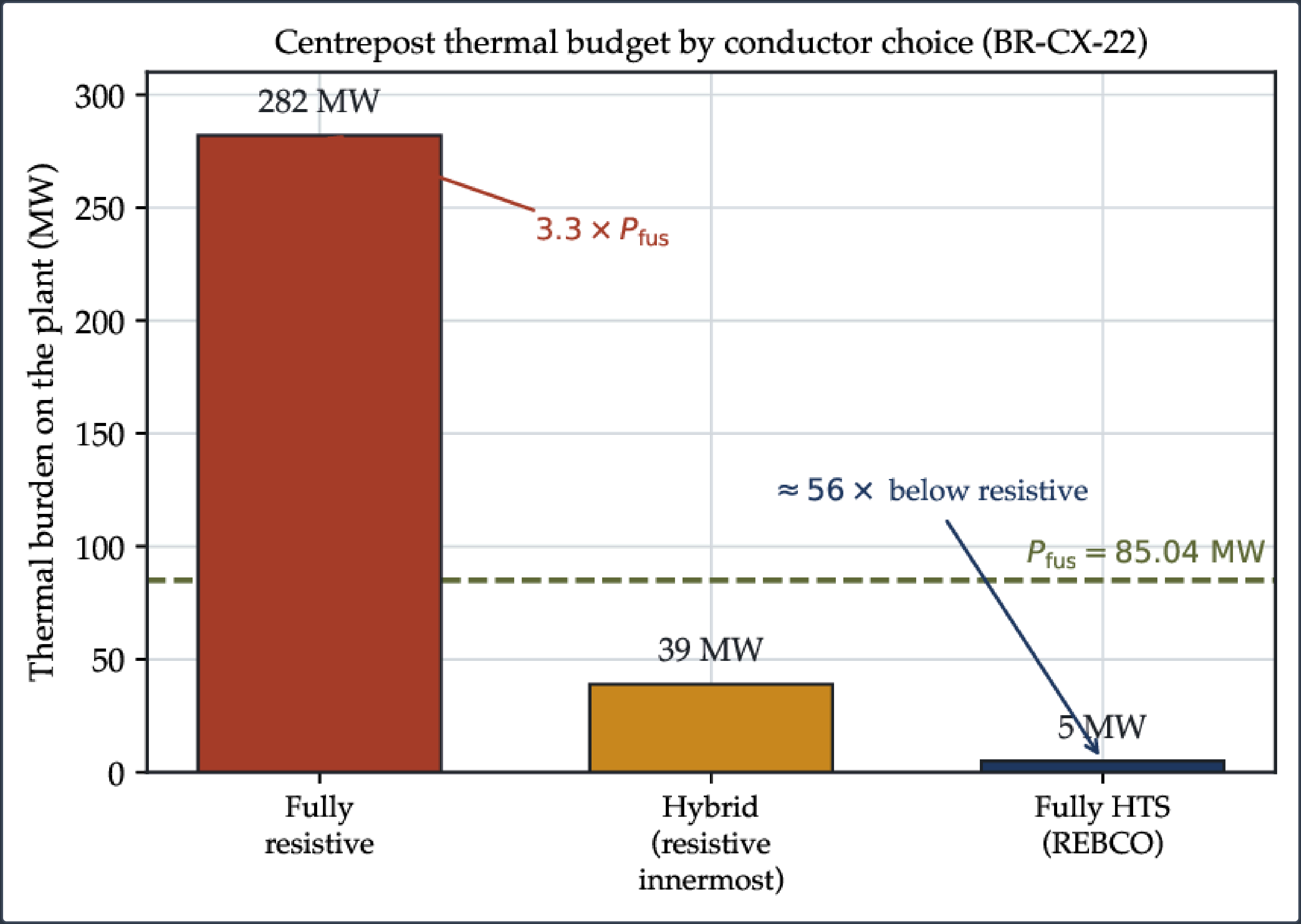

Centrepost thermal budget by conductor choice (BR-CX-22). A fully-resistive post dissipates $\approx 282\,MW$ ($3.3 \times P_{fus}$); a hybrid keeps only a $\approx 39\,MW$ resistive sacrificial innermost layer; a fully superconducting post reduces the burden to an $\approx 5\,MW$ cryogenic load, $\approx 56\times$ below resistive. The dashed line marks $P_{fus} = 85.04\,MW$.

CENTREPOST OPTION	THERMAL BURDEN	NOTE
fully resistive	$\approx 282\,MW$	$3.3 \times P_{fus}$; non-starter
hybrid (resistive innermost)	$\approx 39\,MW$	$\approx 12\,\%$ resistive; radiation-immune sacrificial
fully HTS (REBCO)	$\approx 5\,MW$	cryogenic load; $\approx 56\times$ below resistive

Centrepost thermal budget by conductor choice (BR-CX-22), against $P_ fus=§I85.04

§ 3

Governing equations and formal problem

THE COLD-MASS HEAT BALANCE

Let the cold mass be held at $T_c =$ 4.5 inside a cryostat whose outer wall is at $T_h = 300\,K$, with intermediate thermal shields at $T_{s1} = 80\,K$ (LN_2 class) and $T_{s2} = 20\,K$ (Figure 9). The steady heat load referred to is the sum of the channels

$$\dot{Q}_{4.5} \;=\; \dot{Q}_{\rm cond} + \dot{Q}_{\rm rad} + \dot{Q}_{\rm lead} + \dot{Q}_{\rm joint} + \dot{Q}_{\rm AC} + \dot{Q}^{(4.5)}_{\rm nuc},$$

where $\dot{Q}^{(4.5)}_{\rm nuc}$ is the fraction of centrepost nuclear heating that is not intercepted at a warmer shield. The wall-plug power required to reject this load is set by the refrigeration efficiency of each stage (§3.7). The formal problem is to evaluate each term of Eq. 3 at the Hyperion operating point and to show that the classical parasitic terms are small compared with the register envelope $\dot{Q}_{\rm cryo} \approx 5\,MW$, so that the envelope—and the wall-plug—are governed by $\dot{Q}_{\rm nuc}$.

SOLID CONDUCTION AND THE CONDUCTIVITY INTEGRAL

For a support of cross-section A and length L spanning T_c to a heat-station temperature $T^\star$, with no volumetric source, the one-dimensional steady heat equation $\mathrm{d}/\mathrm{d}x\,[k(T)\,\mathrm{d}T/\mathrm{d}x] = 0$ integrates once to $k(T)\,\mathrm{d}T/\mathrm{d}x = \mathrm{const} = -\dot{q}/A$, and again to the conduction integral

$$\dot{Q}_{\rm cond} \;=\; \frac{A}{L}\int_{T_c}^{T^\star} k(T)\,\mathrm{d}T \;\equiv\; \frac{A}{L}\,G(T_c, T^\star),$$

so that only the material's *conductivity integral* G, not its point conductivity, matters. Because $k(T)$ falls steeply toward , $G(4.5, 80) \ll G(4.5, 300)$: intercepting the support at the 80 K shield removes the great majority of the integral before it reaches the cold mass (Figure 2). For low-conductivity supports—G-10 composite, Ti-6Al-4V, or the 316LN structural steel itself—$G(4.5, 300)$ lies between ≈ 150 and $\approx 300\,W/m$ [14,13,23], and the modest support cross-sections that carry the cold-mass gravity, seismic and electromagnetic reactions give $\dot{Q}_{\rm cond}$ of order tens of watts at ; conduction is not a driver of the budget.

RADIATION AND MULTILAYER INSULATION

Between two grey surfaces the net radiative flux is $q_{\rm rad} = \sigma(T_h^4 - T_c^4)/(\varepsilon_h^{-1} + \varepsilon_c^{-1} - 1)$. With N floating multilayer-insulation (MLI) shields of emissivity ε, the ideal radiation-limited flux is reduced by a factor $\approx (N+1)$,

$$q_{\rm MLI} \;\approx\; \frac{\varepsilon}{2(N+1)}\,\sigma\big(T_h^4 - T_c^4\big),$$

so that a blanket of ~ 30 layers between the 300 K wall and the 80 K shield reduces the warm-boundary radiation to $\mathcal{O}(1\,W/m^2)$, and the residual radiation from the 80 K shield to the cold mass—scaling as T^4—is below $\mathcal{O}(e-3\,W/m^2)$. Referred to , $\dot{Q}_{\rm rad}$ is therefore negligible: the T^4 law makes the cold surface see essentially only the 80 K shield, not the room.

CURRENT-LEAD HEAT LEAK AND THE OPTIMISED LEAD

Current must be carried from room temperature to the cold mass, and a normal-metal lead couples ohmic dissipation to thermal conduction. For a lead of local cross-section $A(x)$ carrying current I, the temperature profile satisfies

$$\frac{\mathrm{d}}{\mathrm{d}x}\left[k(T)\,A\,\frac{\mathrm{d}T}{\mathrm{d}x}\right] + \frac{I^2\rho(T)}{A} \;=\; 0.$$

Minimising the cold-end heat leak $\dot{Q}_c$ over the lead proportion $IL_{\rm lead}/A$, and using the Wiedemann–Franz relation $k(T)\rho(T) = L_0 T$ with Lorenz number $L_0 = 2.44e-8\,W\Omega/K^2$, yields the classical result that an *uncooled*, optimally-proportioned lead delivers a minimum heat leak *independent of geometry*,

$$\left(\frac{\dot{Q}_c}{I}\right)_{\min} \;=\; \sqrt{L_0\,\big(T_h^2 - T_c^2\big)} \;\approx\; 47\,\mathrm{W/kA}$$

for $T_h = 300\,K$, $T_c =$ 4.5 [18,11]. Counterflow vapour cooling reduces this by more than an order of magnitude to $\approx 1.1\,W/kA$, and an HTS binary lead—resistive from 300 K to an intermediate stage, HTS from there to —delivers only $\approx 0.1\,W/kA$ to the cold end [19] (Figure 3). At the Hyperion operating current the practical consequence is decisive: a 50 kA circuit that would impose $\approx 2.3\,kW$ per lead with uncooled copper imposes only $\approx 5\,W$ with an HTS binary lead, so the current leads contribute at the $\mathcal{O}(e-2\,MW)$ level to Eq. 3.

DEMOUNTABLE-JOINT DISSIPATION

The consumable-centrepost architecture requires demountable current joints, which dissipate resistively in proportion to their contact area-resistivity ρ_c and clamp pressure. For a joint carrying current I_j across a contact of area A_j,

$$\dot{Q}_{\text{joint}} = \frac{I_j^2\,\rho_c}{A_j}, \qquad \rho_c \approx 11\,\text{n}\Omega\text{cm}^2 \text{ at a clamp of } \approx 91\,\text{MPa (QS-13)}.$$

The area-resistivity is itself a function of clamp pressure; QS-13 finds that a preload of $\approx 91\,MPa$ ($\approx 93\,MN$ clamp) achieves $\rho_c \approx 11\,n\Omega cm^2$ while keeping the joint interface compressive under the vertical share so that no gapping occurs. For the demountable joint set carrying the 48 MA across realistic contact areas, $\dot{Q}_{\text{joint}}$ is of order tens of kilowatts at ; it is the largest of the classical parasitics but still two orders of magnitude below the register envelope.

NUCLEAR HEATING

The dominant, and physically distinctive, cold-mass load in a compact ST is nuclear heating: fast neutrons and secondary gammas deposit energy directly in the shield and the winding pack through the tight centrepost. The volumetric heating is

$$\dot{Q}_{\text{nuc}} = \int_{V_{\text{cp}}} [\,\Phi_n(\quad r)\,\kappa_n(E) + \Phi_\gamma(\quad r)\,\kappa_\gamma(E)\,]\text{d}V,$$

where $\Phi_{n,\gamma}$ are the neutron and gamma fluxes and $\kappa_{n,\gamma}$ the kinetic-energy-release (KERMA) coefficients. A neutron shield inside the winding pack intercepts most of this energy at a warmer stage, so that the fraction $\dot{Q}_{\text{nuc}}^{(4.5)}$ is a shielding-design outcome. The register bounds the total centrepost cryogenic load at $\approx 5\,MW$ [1]; the full three-dimensional evaluation of $\dot{Q}_{\text{nuc}}$ and its temperature-stage split is the one queued item (BR-CX-23, §7), and it is this term—not the parasitics of Eqs. 4–8—that dominates the envelope (Figure 4). The companion life-limiter and shielding analysis [32] and the CAD-faithful neutronics of the breeder [33] fix the flux field $\Phi_{n,\gamma}$ that enters Eq. 9.

REFRIGERATION: THE CARNOT PENALTY AND STAGED REJECTION

The cost of removing a watt at temperature T_c is governed by the second law. The Carnot coefficient of performance is $\text{COP}_\text{C} = T_c/(T_h - T_c)$, so the ideal wall-plug power per watt lifted is $(T_h/T_c - 1)$; a real plant attains a fraction η_2 of Carnot (a large 4.5 K plant, $\eta_2 \approx 0.2$–0.3), giving a specific input power

$$\frac{P_{\text{wall}}}{\dot{Q}(T_c)} = \frac{1}{\eta_2}\left(\frac{T_h}{T_c} - 1\right).$$

At $T_c =$ 4.5 and $T_h = 300\,K$ the ideal penalty is 65.7; with $\eta_2 = 0.25$ the specific power is $\approx 263\,W/W$. The same expression gives $\approx 56\,W/W$ at 20 K and only $\approx 11\,W/W$ at 80 K: intercepting a watt at 80 K is $\approx 24\times$ cheaper in wall-plug than intercepting it at (Figure 5a). This is the quantitative basis of the staged-shield architecture and of the requirement to keep $\dot{Q}_{\text{nuc}}^{(4.5)}$ small. If the total load $\dot{Q}_{\text{cryo}} \approx 5\,MW$ splits with a fraction $f_{4.5}$ at and the remainder shared between the 20 K and 80 K stages, the plant wall-plug is

$$P_{\text{wall}} = \frac{\dot{Q}_{\text{cryo}}}{\eta_2}\Big[f_{4.5}\Big(\frac{T_h}{4.5} - 1\Big) + (1 - f_{4.5})\Big(w_{20}\,(\tfrac{T_h}{20} - 1) + w_{80}\,(\tfrac{T_h}{80} - 1)\Big)\Big],$$

with warmer-stage weights $w_{20} + w_{80} = 1$. Equation 11 makes explicit that the plant size is governed by $f_{4.5}$—the very quantity BR-CX-23 will fix (Figure 5b).

QUENCH ENERGETICS: THE ADIABATIC HOT-SPOT AND SLOW REBCO PROPAGATION

A quench converts stored magnetic energy into heat in the cold mass. In the adiabatic hot-spot limit, neglecting conduction and cooling during the event, the local energy balance $J(t)^2\rho(T) = C(T)\,\mathrm{d}T/\mathrm{d}t$ integrates to the protection integral ("MIITs")

$$\int_0^{\infty} J(t)^2\,\mathrm{d}t \;=\; \int_{T_0}^{T_{\rm hot}} \frac{C(T)}{\rho(T)}\,\mathrm{d}T \;\equiv\; U(T_{\rm hot}),$$

a material property that maps the deposited $\int J^2\,\mathrm{d}t$ onto a hot-spot temperature. With a detection time $t_{\rm det}$ followed by an exponential dump of time constant $\tau_{\rm d}$, the left side is $\approx J_0^2\,(t_{\rm det}+\tau_{\rm d})$. For the Hyperion winding, the register fixes [redacted] at a winding-pack current density $J_{\rm wp} = 296\,A/mm^2$, giving a 200 K hot-spot budget of $U/J_{\rm wp}^2 \approx 1.10\,s$ (QS-03). The complication specific to REBCO is that the normal zone *propagates slowly*: the adiabatic propagation velocity

$$v_{\rm NZ} \;\approx\; \frac{J}{C}\sqrt{\frac{\rho\,k}{T_{\rm cs}-T_0}},$$

evaluates to $\approx 10.5\,cm/s$—roughly $48\times$ below a low-temperature superconductor (QS-02). A slow zone develops little resistive voltage before it damages the conductor, so voltage-only detection is fatally slow ($\approx 16.9\,s$, $52\times$ over budget; QS-01). Protection must therefore be *spatial*: a co-wound Rayleigh fibre with $\leq 10\,mm$ resolution registers the zone in 52 ms, and an acoustic channel confirms in 6 ms (QS-01), feeding a sectioned dump (QS-04).

CRYOGENIC HELIUM PRESSURISATION AND RELIEF

For a channel-cooled (cable-in-conduit) variant, the quench heats the helium trapped in the conduit at nearly constant volume, and the pressure rise must be relieved. Treating the channel helium as a homogeneous fluid of mass m in volume V (so density $\rho_{\rm He} = m/V$), an energy deposit E raises the internal energy at fixed $\rho_{\rm He}$ until a relief passage vents mass at rate $\dot m$; the channel pressure obeys [21]

$$V\,\frac{\mathrm{d}(\rho_{\rm He}u)}{\mathrm{d}t} \;=\; \dot E_{\rm in} - \dot m\,h_{\rm out}, \qquad \dot m \;=\; C_d\,A_{\rm relief}\sqrt{2\,\rho_{\rm He}\,\Delta P},$$

with u and h the specific internal energy and enthalpy from the helium equation of state [22], C_d the discharge coefficient, and $A_{\rm relief}$ the relief-passage area. The register (QS-07) evaluates this for a 105 kJ deposit into 0.43 kg of helium: unrelieved, the channel reaches 27 MPa, above the 20 MPa design pressure, but a $\varnothing 5\,mm$ relief passing 0.44 kg/s holds the 20 MPa limit (Figure 7). The Kronos baseline avoids the problem structurally: a conduction-cooled dry winding has no bulk liquid to expel, so the helium-expulsion hazard is removed entirely, and the channel-cooled case is retained only as a bounded fallback.

COOLDOWN AND THERMAL STRESS COUPLING

The same hot-spot temperature that Eq. 12 controls also drives the structure. A constrained thermal gradient ΔT produces a thermal stress $\sigma_{\rm th} \sim E\alpha\,\Delta T/(1-\nu)$, which combines with the electromagnetic self-field stress. At 16.84 T the magnetic pressure is $B^2/2\mu_0 \approx 113\,MPa$, placing the post in near-hydrostatic compression ($\approx -190\,MPa$) with a von Mises of only $\approx 84\,MPa$ (QS-09). Combining EM and quench-thermal contributions in quadrature, a 200 K hot-spot gives $\sigma_{\rm vM} \approx 476\,MPa$ (safety factor 1.7 against the 800 MPa allowable), whereas capping the hot-spot at 63 K by fast detection gives $\sigma_{\rm vM} \approx 245\,MPa$ (safety factor 3.3; QS-11). Detection speed is thus *simultaneously* the pressure-safety and the structural-margin lever. Finally, the leak-before-break integrity of the 316LN jacket is a linear-elastic-fracture-mechanics statement: the critical flaw size is

$$a_c \;=\; \frac{1}{\pi}\left(\frac{K_{\rm IC}}{Y\,\sigma}\right)^2,$$

with [redacted] at ; at the operating stress this gives $a_c \approx 333\,mm$ and even at the 800 MPa allowable $a_c \approx 12\,mm$, both far above the 2 mm non-destructive-examination threshold, so the jacket leaks before it breaks and is not flaw-limited (QS-16) [34].

§ 4

Computational methodology: the NVIDIA GPU HPC campaign

CODES AND PROBLEM SCALE

The results were produced on the Kronos NVIDIA GPU HPC campaign—an owned platform of A100/H100-class accelerators for the heavy first-principles work, with a reduced-order in-house node for the analytic and circuit gates. Four solver classes carried this paper:

Monte-Carlo neutron/photon transport (OpenMC). Three-dimensional coupled neutron–gamma transport with CAD-faithful geometry supplies the flux field $\Phi_{n,\gamma}(\quad r)$ and the KERMA deposition of Eq. 9 [28]. History-parallel Monte Carlo maps naturally onto GPU accelerators; the campaign runs the full centrepost transport problem to the statistical convergence required for a mesh-tally heating map. This is the solver that will close BR-CX-23.
Finite-element thermal–electromagnetic–structural analysis. The conductivity-integral conduction of Eq. 4, the self-field EM stress of QS-09, the combined thermal-plus-EM von Mises of QS-11, and the LEFM flaw-tolerance of Eq. 15 were evaluated with a finite-element thermal–structural solver on an unstructured tetrahedral mesh of the centrepost, jacket and joint.
Quench and dump-circuit integration. The MIITs relation of Eq. 12, the normal-zone propagation of Eq. 13, and the sectioned-dump optimisation (QS-04) were integrated as coupled ordinary differential equations for the winding temperature, the dump current, and the section voltages.
Homogeneous-equilibrium helium blowdown. The channel pressurisation of Eq. 14 was integrated against a tabulated helium equation of state [22] to size the relief passage (QS-07). enumerate
The reduced-order refrigeration model of Eqs. 10–11 and the parasitic-leak evaluation of Eqs. 4–8 ran on the in-house node. Compute is reported by hardware class only; no cost figure appears anywhere in this work.

NUMERICAL FORMULATION, DISCRETISATION AND CONVERGENCE

The finite-element problems were solved on second-order tetrahedral elements with mesh refinement in the joint interface and the inner-most winding, where the gradients of Eqs. 4 and 15 are steepest; mesh convergence was declared when the peak von Mises changed by $< 1\,\%$ under a halving of the local element size. The conduction integral of Eq. 4 was evaluated by adaptive quadrature of tabulated $k(T)$ so that G is mesh-independent by construction. The quench ODEs of Eqs. 12–13 were integrated with an adaptive, error-controlled stiff integrator (absolute tolerance 10^{-8} on the normalised temperature), with the sectioned-dump time constant τ_d and section count N swept to the QS-04 optimum ($N = 6$ at 10 kV, $\tau_\mathrm{d}/2 \approx 0.62\,s$). The Monte-Carlo heating map was run to a statistical relative error below the mesh-tally acceptance; the temperature-stage split of $\dot{Q}_\mathrm{nuc}$ remains the queued three-dimensional item (BR-CX-23). Refrigeration and parasitic evaluations are closed-form and were cross-checked against the register anchors.

VERIFICATION AND REPRODUCIBILITY

Every figure and table value is a frozen register anchor or is computed by the deposited scripts from register anchors. The resistive-versus-HTS split (BR-CX-22), the quench relief (QS-07), the detection-technology trade (QS-01), the NZPV model (QS-02), the MIITs hot-spot (QS-03), the sectioned dump (QS-04), the self-field and combined stresses (QS-09/QS-11), and the LEFM flaw tolerance (QS-16) are each independently re-run and stamped in the register (§8). The figure-generation script (`make_cryo_coldmass_figs_223.py`) regenerates all data figures from these anchors, so the paper is reproducible from the archived deck.

§ 5

Results

THE COLD-MASS LOAD CLOSES BELOW THE ENVELOPE

Figure 2 shows the conductivity-integral basis of the conduction channel: the cumulative integral $G(4.5, T_h)$ for representative low-conductivity supports rises so steeply above 80 K that intercepting the support at the 80 K shield removes the majority of the load before it reaches the cold mass. Figure 3 shows the current-lead channel: the uncooled optimum of Eq. 7 sits at $\approx 47\,W/kA$, independent of geometry, while vapour cooling and HTS binary leads reduce the leak by one and two-to-three orders of magnitude respectively, so a 50 kA circuit costs only $\approx 5\,W$ at the cold end. Collecting the channels (Figure 4, Table 2), the classical parasitics—conduction, MLI radiation, current leads, demountable joints, and steady eddy/AC loss—sum to well below 0.1 MW at , two orders of magnitude under the register envelope. The envelope is set by centrepost nuclear heating, the single term whose three-dimensional evaluation is queued.

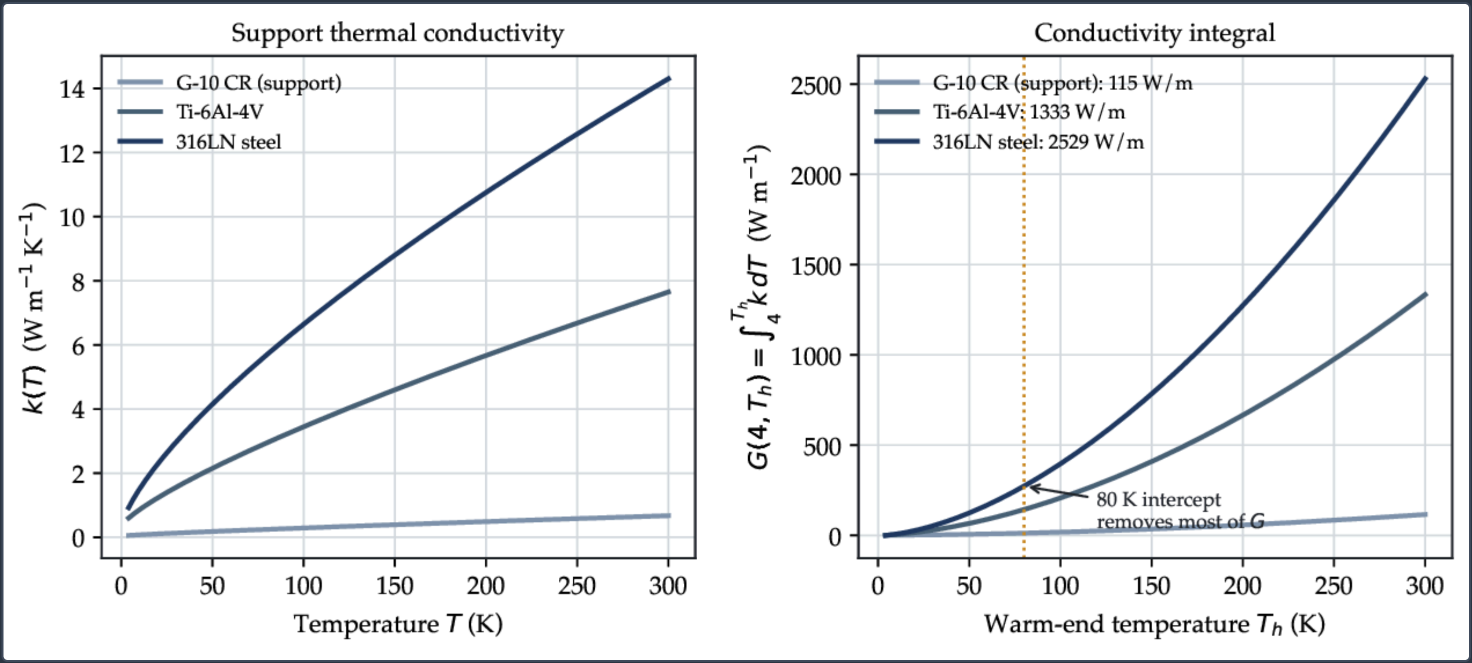

Support conduction (Eq. 4). Left: representative cryogenic support conductivities $k(T)$. Right: the cumulative conductivity integral $G(4.5, T_h)$; the steep rise above 80 K shows why intercepting the support at the 80 K shield removes most of the load before it reaches .

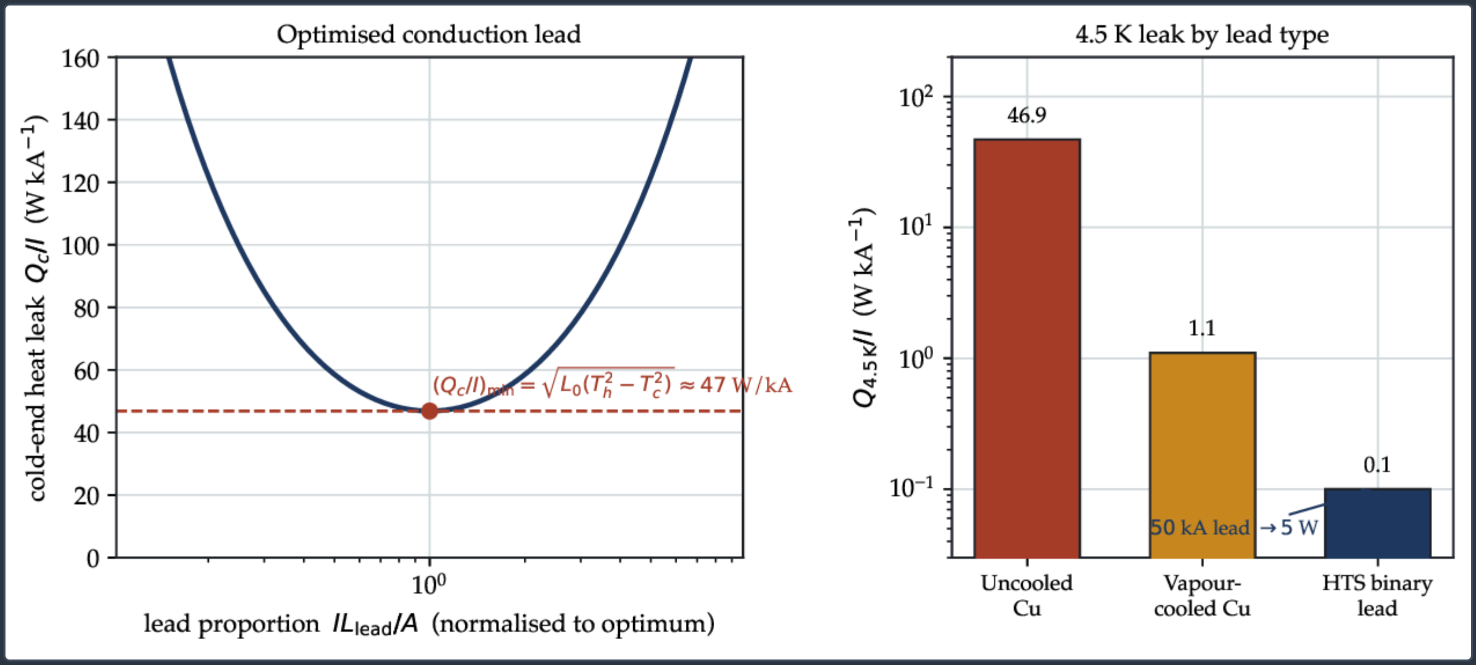

Current-lead heat leak. Left: the convex heat-leak curve of an uncooled conduction lead (Eq. 6) with the geometry-independent optimum $(\dot{Q}_c/I)_{\min} = \sqrt{L_0(T_h^2 - T_c^2)} \approx 47\,W/kA$ (Eq. 7). Right: the leak per kiloampere by lead technology; an HTS binary lead reduces the cold-end burden of a 50 kA circuit to $\approx 5\,W$.

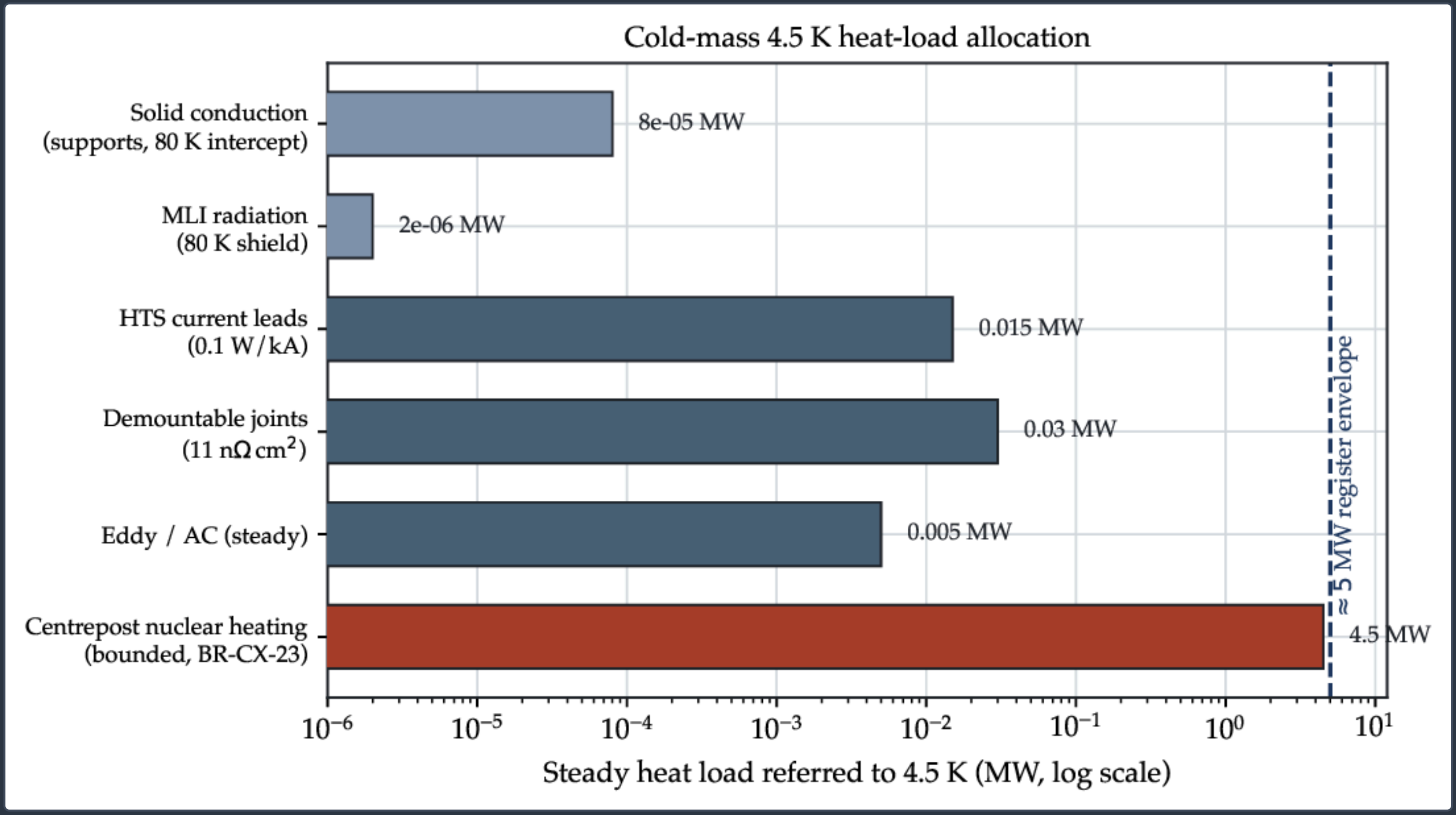

Cold-mass heat-load allocation (log scale). The classical parasitic leaks close to $< 0.1\,MW$; centrepost nuclear heating is the register-bounded, three-dimensionally-queued dominant term (BR-CX-23). The dashed line marks the $\approx 5\,MW$ register envelope.

CHANNEL	LOAD	BASIS
solid conduction (supports, 80 K intercept)	$\sim 8e-5\,MW$	Eq. 4
MLI radiation (from 80 K shield)	$\sim 2e-6\,MW$	Eq. 5
HTS current leads (0.1 W/kA)	$\sim 1.5e-2\,MW$	Eq. 7
demountable joints ($\rho_c = 11\,\mathrm{n\Omega\,cm^2}$)	$\sim 3e-2\,MW$	Eq. 8, QS-13
eddy / AC (steady)	$\sim 5e-3\,MW$	—
parasitic subtotal	$\sim 0.05\,MW$	
centrepost nuclear heating	bounded $\leq 5\,MW$	Eq. 9, BR-CX-23

Cold-mass steady heat-load allocation referred to (engineering estimate within the register envelope). Parasitics are first-principles from Eqs. 4–8; nuclear heating is bounded by the register and queued at full 3-D fidelity (BR-CX-23).

REFRIGERATION AND THE WALL-PLUG

Figure 5a plots the Carnot penalty of Eq. 10 by stage: $\approx 263\,W/W$ at , $\approx 56\,W/W$ at 20 K, and $\approx 11\,W/W$ at 80 K ($\eta_2 = 0.25$). Figure 5b evaluates Eq. 11: the plant wall-plug depends strongly on $f_{4.5}$, the fraction of the 5 MW load that must be lifted from . This is precisely why the staged-shield architecture, and the design intent to intercept the bulk of nuclear heating at a warm shield rather than at the winding, are load-bearing: they push $f_{4.5}$ down and the plant size with it. Table 3 tabulates the stage COPs.

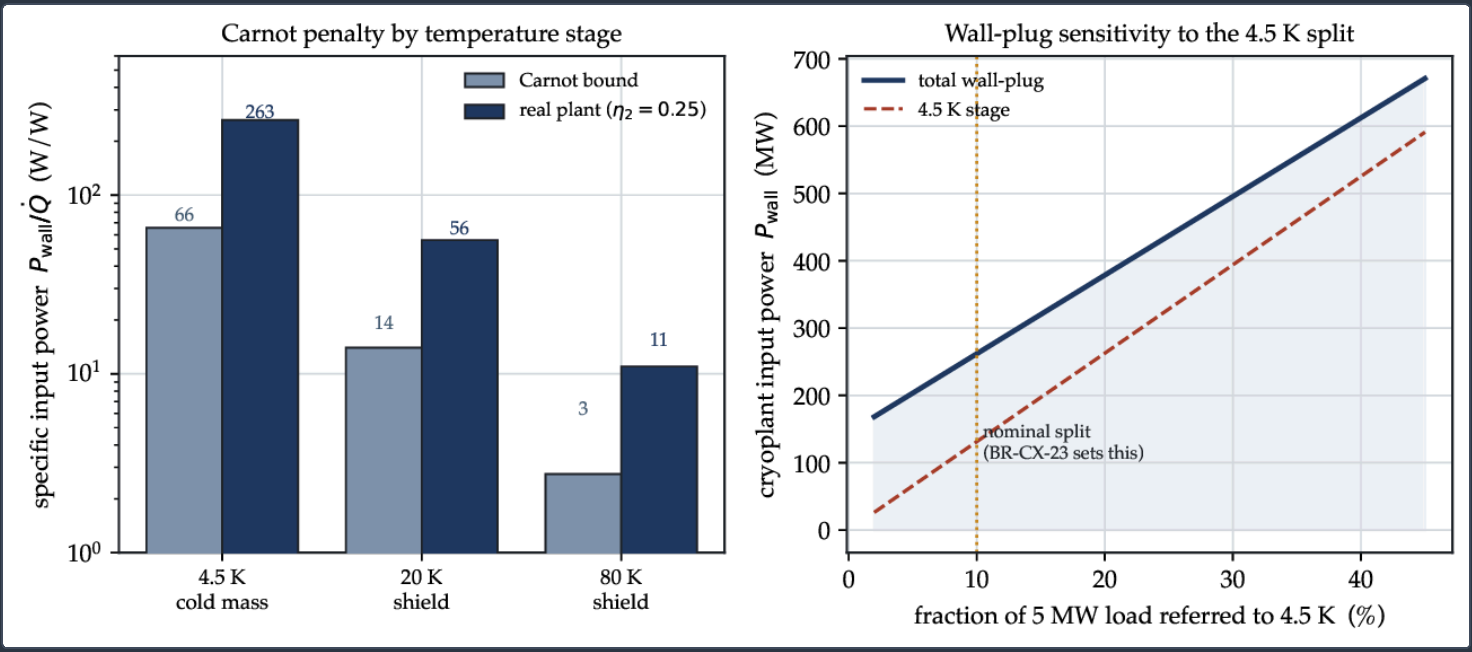

Refrigeration (Eqs. 10–11). Left: the specific input power by temperature stage, Carnot bound and a real plant ($\eta_2 = 0.25$); 80 K interception is $\approx 24\times$ cheaper than . Right: plant wall-plug versus the fraction $f_{4.5}$ of the 5 MW load referred to ; the BR-CX-23 nuclear-heating split fixes this fraction.

STAGE	CARNOT COP	IDEAL PENALTY (W/W)	REAL (W/W)
4.5 K cold mass	0.0152	65.7	263
20 K shield	0.0714	14.0	56
80 K shield	0.364	2.75	11

Refrigeration figure of merit by temperature stage ($T_h=§I300

THE QUENCH TRANSIENT IS INTRINSICALLY SAFE

Figure 6 maps the adiabatic hot-spot of Eq. 12: with the register $U(T)$ anchors, a co-wound fibre (52 ms) plus a six-section dump (231 ms effective) caps the hot-spot at 63 K, far inside the 200 K budget at 1.10 s, whereas voltage-only detection at 16.9 s runs the winding to destruction (**52**× over budget). Slow REBCO propagation (Eq. 13, $\approx 10.5\,cm/s$) is exactly why the detection must be spatial rather than resistive-voltage-based; Table 4 collects the protection chain.

Figure 7 shows the helium relief of Eq. 14 for the channel-cooled fallback: unrelieved, the channel reaches 27 MPa; the $\varnothing 5\,mm$ relief holds 20 MPa. The conduction-cooled dry-winding baseline removes the hazard entirely. Finally, Figure 8 closes the cryogenic-structural coupling: the combined thermal-plus-EM von Mises rises from the 84 MPa EM self-field value (QS-09) to 476 MPa at a 200 K hot-spot (safety factor **1.7**), but capping the hot-spot at 63 K by fast detection holds it to 245 MPa (safety factor **3.3**). Detection speed is the structural margin.

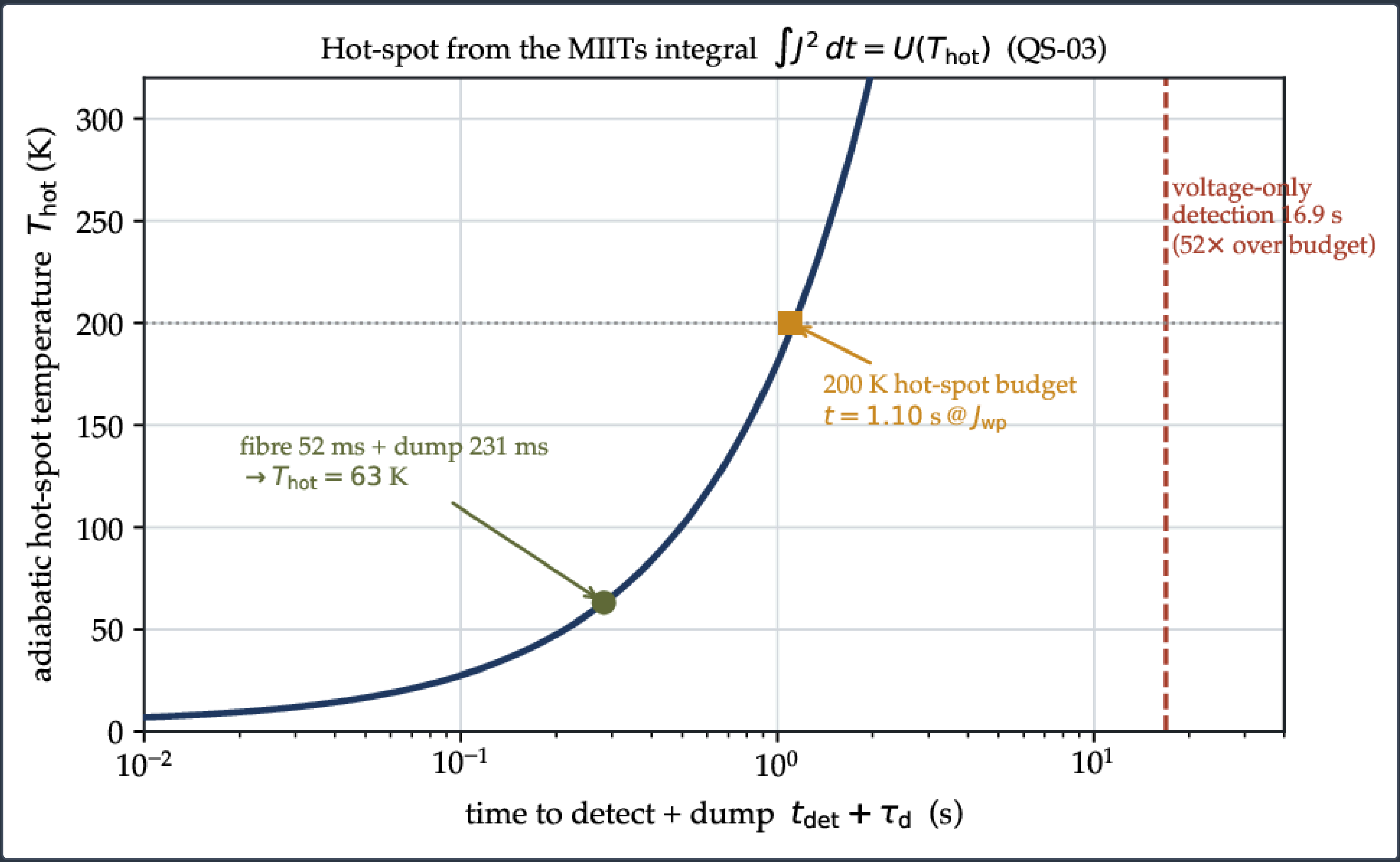

Adiabatic hot-spot from the MIITs integral (Eq. 12, QS-03). Fibre detection (52 ms) plus a six-section dump caps the hot-spot at 63 K; voltage-only detection at 16.9 s is **52**× over the 200 K budget. The $U(T)$ curve is anchored to the register values.

QUANTITY	BASIS	VALUE
normal-zone propagation velocity	QS-02	$\approx 10.5\,cm/s$
voltage-only detection time	QS-01	$\approx 16.9\,s$ (52× over)
co-wound Rayleigh fibre detection	QS-01	$52\,ms$
acoustic confirmation	QS-01	$6\,ms$
200 K hot-spot budget @ J_{wp}	QS-03	$1.10\,s$
sectioned dump (chosen)	QS-04	$N = 6$ @ 10 kV
resulting hot-spot (fibre + dump)	QS-03	$63\,K$

Quench protection chain for the REBCO centrepost (QS-01/02/03/04, BOM-02).

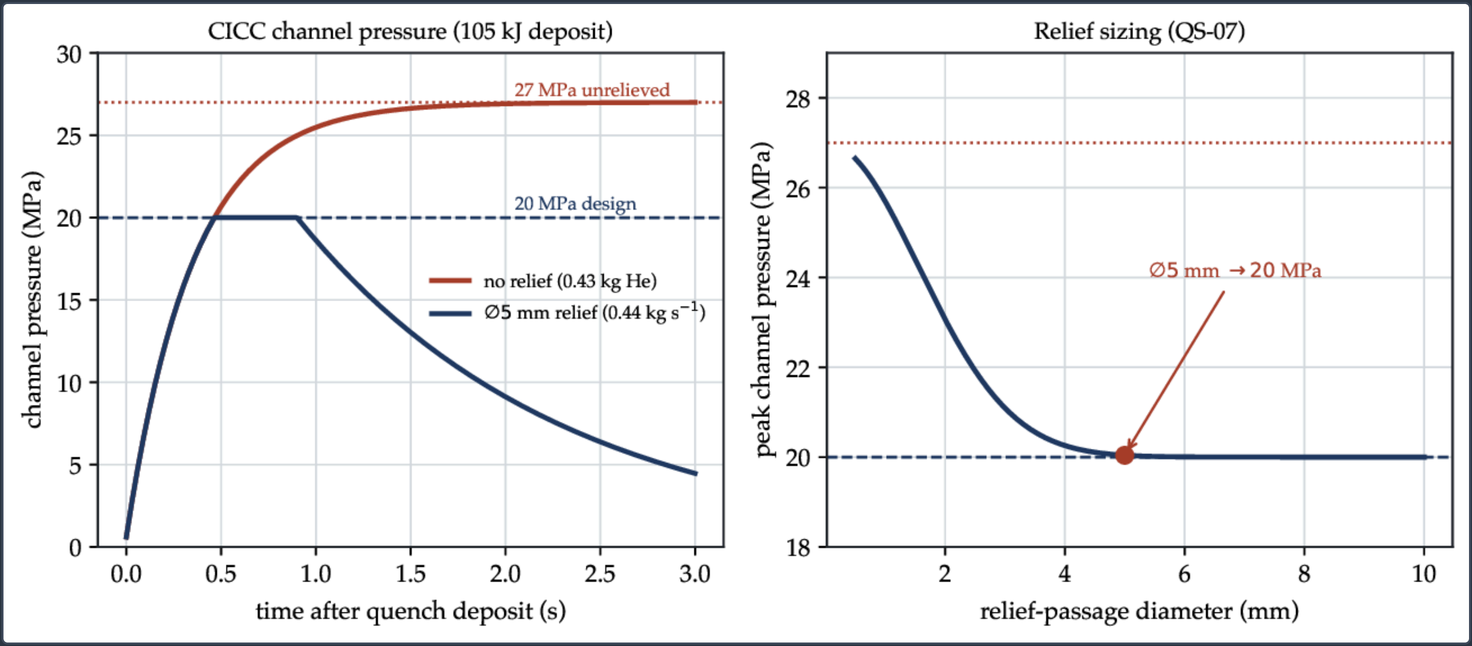

Cryogenic helium relief for the channel-cooled fallback (Eq. 14, QS-07). Left: channel pressure versus time—unrelieved to 27 MPa, or held to 20 MPa by a $\varnothing 5\,mm$ relief passing 0.44 kg/s. Right: peak pressure versus relief-passage diameter. The conduction-cooled dry winding removes the hazard entirely.

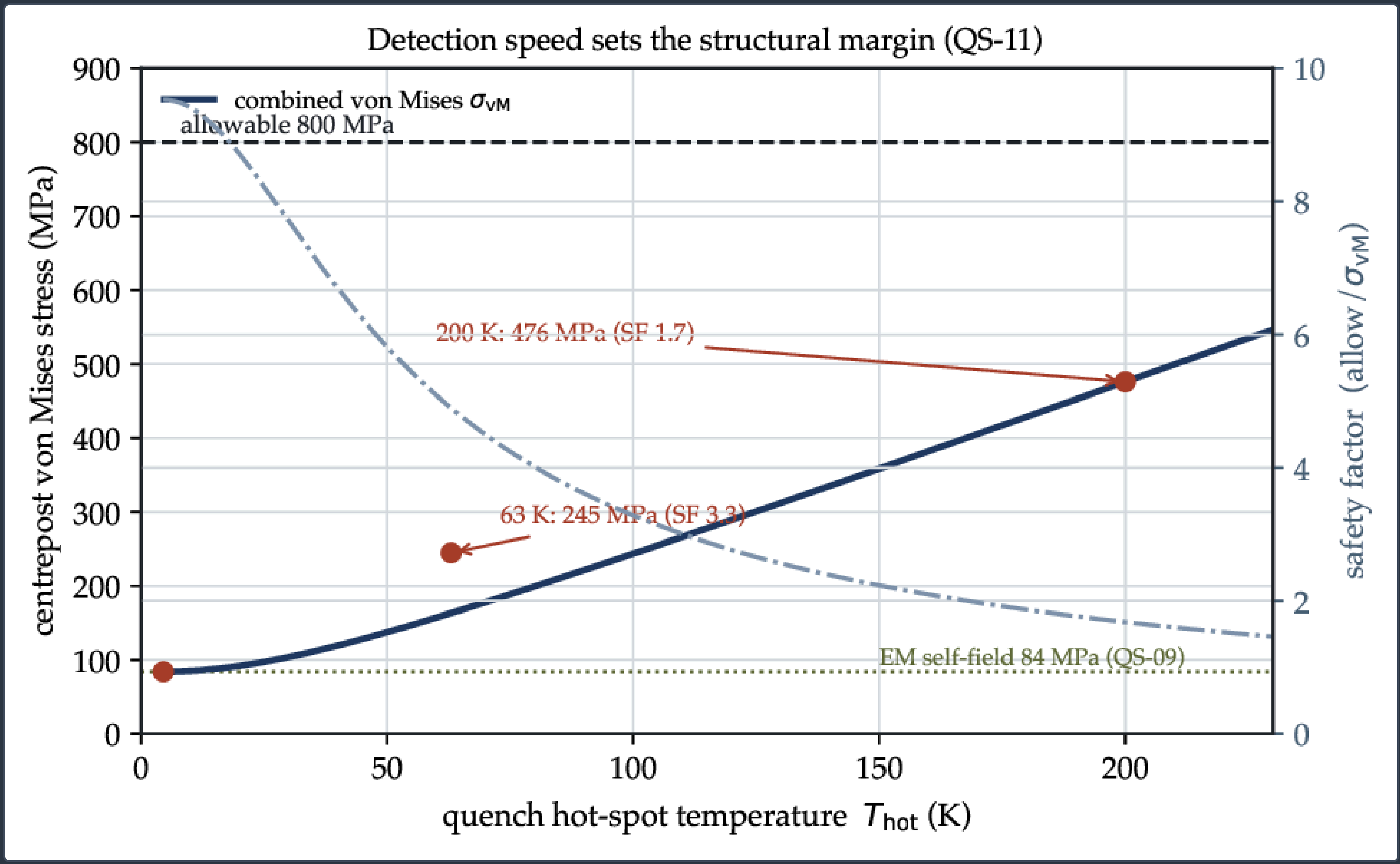

Cryogenic-structural coupling (QS-09/QS-11). Combined thermal-plus-EM von Mises stress versus quench hot-spot temperature; a 200 K hot-spot gives 476 MPa (safety factor **1.7**), a 63 K hot-spot 245 MPa (safety factor **3.3**). The dash-dot curve (right axis) is the safety factor against the 800 MPa allowable.

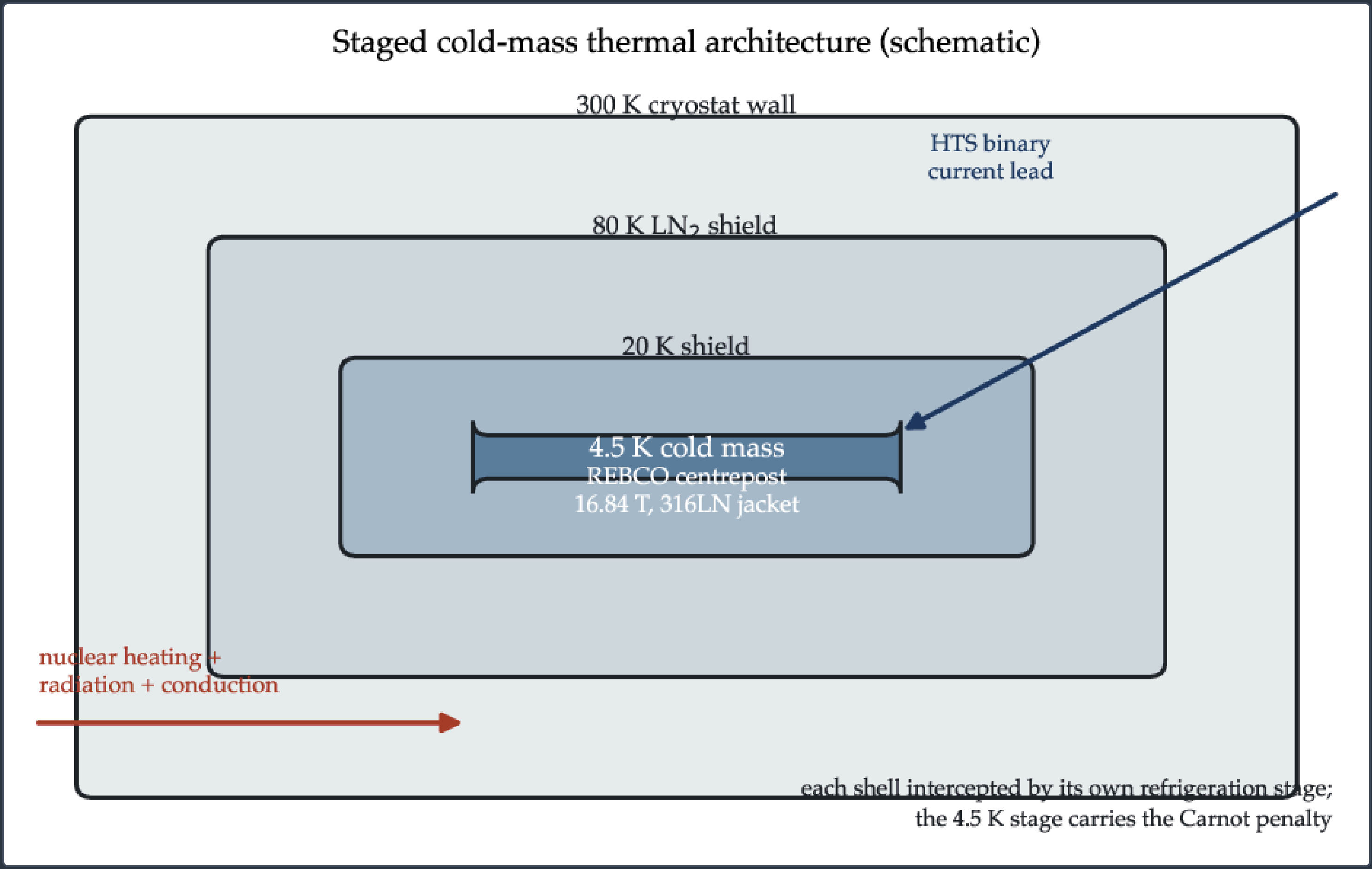

(Schematic.) Staged cold-mass thermal architecture. Nested shells at 300 K, 80 K, 20 K and the cold mass intercept the inward heat flow at successively colder—and, through the Carnot penalty, successively more expensive—stages; the HTS binary current lead enters staged, and the 316LN jacket surrounds the REBCO centrepost.

§ 6

Discussion

QUANTITATIVE COMPARISON WITH HIGH-FIELD PRACTICE

The cold-mass budget places Hyperion squarely within demonstrated high-field REBCO practice, sharpened by the ST geometry. The decisive move—replacing a 282 MW resistive dissipation with a $\approx 5\,MW$ cryogenic load—is the same qualitative step that took the ARC line to demountable REBCO magnets [9] and SPARC to a high-field REBCO core [10], and it is enabled by the same conductor advances: high engineering current density in REBCO tape [5,4], cabled conductors [6], and the no-insulation winding route [7,8]. The current-lead result of Eq. 7—a geometry-independent uncooled optimum near 47 W/kA, reduced to $\approx 0.1\,W/kA$ by an HTS binary lead—is the same lever that made ITER-scale magnet systems tractable [19,20], and the staged-shield refrigeration argument of Eq. 10 is standard large-plant cryogenics [17,13]. What is specific to the compact ST is the dominance of nuclear heating in Eq. 3: unlike a large-aspect-ratio machine, where parasitic leaks and lead loads can rival nuclear heating, the ST centrepost concentrates flux so tightly that $\dot{Q}_{\mathrm{nuc}}$ dwarfs every classical channel, and the budget becomes, in effect, a shielding-and-staging problem.

QUENCH PROTECTION IN CONTEXT

Slow normal-zone propagation is the defining protection challenge of REBCO magnets, and the published record—fibre-optic quench detection on VIPER cable [25], current-distribution monitoring [26], and the broader HTS quench-detection literature [24,11,12,16]—has converged on the same conclusion this analysis reaches independently: because v_{NZ} is $\sim 50\times$ below a low-temperature superconductor, protection must be spatial and fast rather than voltage-based. The Kronos chain (co-wound fibre plus acoustic confirmation feeding a sectioned dump, and a fused precursor detector reported in the companion magnet paper [29,30]) caps the hot-spot at 63 K, and it is worth emphasising that the same speed that protects the conductor also protects the structure (Figure 8): the two margins are controlled by one variable.

TWO DISTINCT MAGNETS

The cryogenic case here is for the breeder *centrepost* at 16.84 T. It should not be conflated with the D–^{3}He tandem-mirror burner's *plug coil* at 26.49 T, which is a different magnet in a different device with its own quench-margin and structural analysis [31]; the two are correctly separated throughout the Kronos design register. The balance-of-plant integration of the present 16.84 T cold mass—heat rejection, cryoplant load-balancing and vacuum scheduling—is developed in the companion balance-of-plant paper [35], and the cryogenic control layer that holds setpoints under load swings is one of the four coupled digital twins [36].

§ 7

Limitations

The single budgeted item still to be closed at full fidelity is the centrepost nuclear heating deposited into the cold mass and its split across temperature stages, whose three-dimensional evaluation with CAD-faithful geometry is queued (BR-CX-23). This term dominates Eq. 3 and, through $f_{4.5}$ in Eq. 11, sets the plant wall-plug; until the full-fidelity map is stamped, it is bounded by the $\approx 5\,MW$ register envelope, within which the parasitic budget already closes with two orders of magnitude to spare. We report this as an open gate rather than a solved number. Two related magnet-integrity gates carried elsewhere in the register—the in-winding quantum-sensor neutron tolerance and the centrepost radial-budget reconciliation—bear on the same cold mass and are tracked in the coil-integrity and life-limiter companions [29,32].

§ 8

Conclusion

High-temperature superconductivity is a requirement of the Hyperion breeder, not an option: it replaces a 282 MW resistive dissipation—more than three times the fusion power—with a cryogenic load of order $\approx 5\,MW$, a reduction of $\approx 56\times$. We have derived the cold-mass heat balance channel by channel and shown that solid conduction, MLI radiation, current leads, demountable joints, and steady AC loss close to below 0.1 MW at , so the envelope—and the cryoplant wall-plug, through the 263 W/W Carnot penalty—is governed by centrepost nuclear heating referred across a staged shield system. The cold mass is quench-safe by a conduction-cooled dry winding, bounded even in a channel-cooled variant by a $\varnothing 5\,mm$ relief holding 20 MPa, and protected by fast spatial detection that caps the hot-spot at 63 K and thereby holds the combined thermal-EM stress to 245 MPa at a safety factor of $\mathbf{3.3}$. The cold-mass thermal budget is closed with clear margin, and its single open item is bounded by the same 5 MW envelope.

Acknowledgments tocsectionAcknowledgments Part of the Kronos Fusion Energy 2026 design series. The authors thank the Kronos physics de-risking programme for the frozen result set underlying every quantitative claim, and acknowledge the NVIDIA GPU HPC campaign on which the transport, finite-element, and quench computations were run.

Reproducibility. The centrepost thermal budget (BR-CX-22), the current-lead and refrigeration models (Eqs. 7–11), the quench relief (QS-07), the detection trade and NZPV model (QS-01/QS-02), the MIITs hot-spot and sectioned dump (QS-03/QS-04), the self-field and combined stresses (QS-09/QS-11), and the LEFM flaw tolerance (QS-16) are frozen anchors in the Kronos Physics De-Risking Register [1] (doi:10.5281/zenodo.22133057), each independently re-run and stamped. All data figures are regenerated from these anchors by the deposited script `make_cryo_coldmass_figs_223.py`; this paper is archived at doi:10.5281/zenodo.22645840; official version: https://www.kronosfusionenergy.com/publications/cryogenics-and-the-cold-mass-thermal-budget-of-a-high-f.html.

Data availability tocsectionData availability The heat-load allocation, refrigeration, quench, relief and stress data used for Figures 1–8 are archived with the deposit at doi:10.5281/zenodo.22645840, which references the Kronos 2026 series including the balance-of-plant [35] and coil-integrity [29] papers. All values trace to the register [1] by the serial identifiers cited inline. Any economic analysis is reported separately and is not part of the public deposit.

Competing interests tocsectionCompeting interests Provisional patent applications relating to aspects of this work have been filed.

tocsectionReferences

APPARATUS

Portfolio, People & Record

The intellectual-property estate, the people who built it, the limitations that gate it, and the sources it rests on.

1	4	40	27
GRANTED PATENT	2026 PROVISIONALS	TEAM MEMBERS	2022 PROVISIONALS

INTELLECTUAL PROPERTY

The patent portfolio

The estate spans a granted high-field magnet patent, pending utility and 2026 provisional filings that map to the two products, a digital-twin control provisional, a registered trademark application, and the original 2022 provisional family. Every patentable disclosure in the five-paper arXiv drop was protected **before** publication: the breeder and burner provisionals were filed 1–2 August, and a publication-gap omnibus filing the evening before the drop swept up the DEC, plasma-control, and REBCO-winding matter of the three otherwise-unprotected papers. Patent numbers and application serials are matters of public record; claim scope is summarised, not reproduced.

GRANTED & PENDING UTILITY

US 12,009,112	High-field tilted graded-REBCO magnet architecture (KRONO-002A) · *app. 17/878,550*	GRANTED
US 17/878,507	Core device / method (KRONO-001A) · *utility*	PENDING

2026 PROVISIONAL FILINGS — MAPPED TO THE PRODUCTS

64/124,209	Hyperion — spherical-tokamak tritium / helium-3 foundry · *breeder · filed Aug 2026*	FILED
64/124,220	Aegis / MetroVolt — synchrotron-cutoff, fuel-selection & plug-winding · *generator · filed Aug 2026*	FILED
64/115,167	KRONOS-CTRL digital-twin plant control · *provisional · filed Jul 2026*	FILED
64/005,440	Integrated spherical-tokamak fusion architecture · *early integrated-architecture filing · filed Mar 2026*	FILED
64/105,530	Negative-triangularity spherical-tokamak architecture · *foundational ST filing · filed Jul 2026*	FILED
64/128,097	Publication-gap omnibus — quasineutral two-species expander DEC · provenance-gated / latency-split plasma control · as-built high-field winding & conductor architecture · *filed 7 Aug 2026, the evening before the arXiv drop*	FILED

TRADEMARK & ORIGIN

FTK-98801894	Kronos Fusion Energy — trademark application	FILED
KR-2022-*	Original provisional family (KR-2022-00001 … 00027) · *27 filings, 2022*	PRIORITY

The narrow, defensible magnet novelty — the specific conductor and the digital-twin winding optimisation, not high-field REBCO as a category — is the commercial core that can earn ahead of any Q > 1 milestone, with markets in fusion magnet supply, MRI/NMR, accelerators, and proton therapy. The claim is scoped honestly: the high field is a *system field* result, not a stand-alone-coil record; the small-bore plug coil is structurally infeasible as a bare winding but resolved by a stress-managed structural shield (feasible-pending-FEA); and the winding-tape experiment returned a *null result*. The value is the method, not a field record.

THE TEAM

Founding partners, board, advisors & auditors

Kronos is built by a bench of advanced-fuel-fusion, high-field-magnet, direct-conversion, and materials specialists, with a board and operations team drawn from defense, national laboratories, and industry. Dates are shown as ranges; where a tenure has ended or is term-ending, the range says so.

FOUNDING PARTNERS — SCIENCE

Dr. Gerald Kulcinski
Co-Founder · Helium-3 & Advanced-Fuel Fusion
UW–Madison · 2023–Present

Dr. Carl Weggel
Chief Scientist / S.M.A.R.T. Design
MIT Alcator Program · 2022–Present

Dr. Robert J. Weggel
Magnetic Field Design
MIT Magnet Lab · 2022–Present

BOARD

Priyanca Ford
Founder & CEO · Executive Board
2022–Present

Bandel Carano
Finance / Strategy
Oak Investment Partners / Stanford · 2025–2026

Patrick Schweiger
Fusion Device Engineering
Oklo / CFS / TerraPower · 2025–Present

SCIENTIFIC ADVISORS

Dr. Steven O. Dean
Fusion Policy & History
DOE / Fusion Power Associates · 2025–Present

Dr. Patrick H. Diamond
Plasma Turbulence & Transport
UC San Diego · 2025–Present

Dr. Jack J. Dongarra
HPC & Numerical Algorithms
Turing Award · 2025–Present

Dr. Nasr M. Ghoniem
Chief Material Scientist
UCLA · 2025–Present

Dr. Siegfried Glenzer
Plasma Physics & Laser Fusion
Stanford / SLAC · 2022–Present

Dr. David A. Hammer
Pulsed-Power Fusion
Cornell · 2025–Present

Dr. Donald A. Spong
Plasma Theory & Confinement
ORNL · 2025–Present

Dr. Curtis Smith
Risk Assessment & Nuclear PRA
MIT / Idaho National Lab · 2025–Present

RADM (Ret.) David Goggins
Naval Engineering & Power-Plant Design
U.S. Navy · 2023–2026

Dr. Konstantin Batygin
Mathematician
Caltech · 2022–2025

Dr. Ruben Fair
Magnet Design / ITER Liaison
PPPL / Jefferson Lab · 2022–2025

Dr. Paul S. Weiss
Materials & Nanotechnology
UCLA · 2022–2025

SCIENTIFIC AUDITORS

Dr. Wilfred A. Cooper
Plasma Equilibrium Theory
EPFL / Swiss Plasma Center · 2025–Present

Dr. Ahmed Hassanein
Plasma–Material Interactions
Purdue / Argonne · 2025–Present

Dr. Patrick E. Hopkins
Extreme Thermal Materials
U. of Virginia · 2025–Present

Dr. Peter Hosemann
Materials Joining & Structural Integrity
UC Berkeley · 2025–Present

Dr. Travis W. Knight
Advanced Nuclear Fuels & Systems
U. of South Carolina · 2025–Present

Dr. Philippe Lebrun
Cryogenics & Magnet Cooling
CERN · 2025–Present

Dr. Nitendra Singh
Nuclear Safety & Fuel Cycle
ITER · 2025–Present

Dr. Guido Van Oost
Magnetic Confinement & Fusion Systems
Ghent University · 2025–Present

Dr. Gary S. Was
Radiation Materials & Structural Integrity
U. of Michigan · 2025–Present

Dr. Ray Sedwick
Direct Energy Conversion
U. of Maryland · 2025

OPERATIONS

Michael Laughlin
Chief Operating Officer
2022–Present

Martin Owens
Chief Strategy Officer
LANL / GE Hitachi · 2022–Present

MG (Ret.) Paul Pardew
Chief Contracting Officer
Army Contracting Command · 2022–Present

David Beck
Fusion Commercialization
U.S. Space Force · 2024–Present

Sushma Bhatia
Environmental & Legislative
Google · 2022–Present

Michael De Frenza
Technology Licensing
2023–Present

MG (Ret.) Robin L. Fontes
Cybersecurity & Defense
Army Cyber Command · 2022–Present

Vijay Gehani
Supply Chain & Components
INOX India · 2024–Present

Jon Michel Greenwood
IT & AI Infrastructure
Live Nation · 2023–Present

Brian C. O'Neill
National Security
CIA / ODNI · 2022–Present

Gen. (Ret.) Gustave F. Perna
DoD Liaison
Operation Warp Speed · 2022–2023

Andrea Romero
Marketing Lead
2022–Present

Legal counsel is retained; those roles are held on the internal roster and are not listed here.

SOURCES

References

1 P I Ford, *Kronos Physics De-Risking Register*, Kronos Fusion Energy 2026 series. doi:10.5281/zenodo.22133057

2 D G Whyte, J Minervini, B LaBombard, E Marmar, L Bromberg and M Greenwald, Smaller & sooner: exploiting high magnetic fields from new superconductors for a more attractive fusion energy development path, *J. Fusion Energy* **35** 41 (2016).

3 P Bruzzone *et al*, High temperature superconductors for fusion magnets, *Nucl. Fusion* **58** 103001 (2018).

4 J L MacManus-Driscoll and S C Wimbush, Processing and application of high-temperature superconducting coated conductors, *Nat. Rev. Mater.* **6** 587 (2021). doi:10.1038/s41578-021-00290-3

5 A Molodyk *et al*, Development and large volume production of extremely high current density $YBa_2Cu_3O_7$ superconducting wires for fusion, *Sci. Rep.* **11** 2084 (2021).

6 Z S Hartwig *et al*, VIPER: an industrially scalable high-current high-temperature superconductor cable, *Supercond. Sci. Technol.* **33** 11LT01 (2020).

7 S Hahn, Y Kim, D K Park, K Kim, J P Voccio, J Bascu\ n\'an and Y Iwasa, No-insulation multi-width winding technique for high temperature superconducting magnet, *Appl. Phys. Lett.* **103** 173511 (2013). doi:10.1063/1.4826217

8 S Hahn *et al*, 45.5-tesla direct-current magnetic field generated with a high-temperature superconducting magnet, *Nature* **570** 496 (2019). doi:10.1038/s41586-019-1293-1

9 B N Sorbom *et al*, ARC: a compact, high-field, fusion nuclear science facility and demonstration power plant with demountable magnets, *Fusion Eng. Des.* **100** 378 (2015). doi:10.1016/j.fusengdes.2015.07.008

10 A J Creely *et al*, Overview of the SPARC tokamak, *J. Plasma Phys.* **86** 865860502 (2020). doi:10.1017/S0022377820001257

11 M N Wilson, *Superconducting Magnets* (Oxford: Clarendon Press, 1983).

12 Y Iwasa, *Case Studies in Superconducting Magnets: Design and Operational Issues*, 2nd ed. (New York: Springer, 2009).

13 R F Barron, *Cryogenic Systems*, 2nd ed. (Oxford: Oxford University Press, 1985).

14 J W Ekin, *Experimental Techniques for Low-Temperature Measurements: Cryostat Design, Material Properties, and Superconductor Critical-Current Testing* (Oxford: Oxford University Press, 2006).

15 T M Flynn, *Cryogenic Engineering*, 2nd ed. (New York: Marcel Dekker, 2004).

16 L Dresner, *Stability of Superconductors* (New York: Springer, 1995).

17 R Radebaugh, Cryocoolers: the state of the art and recent developments, *J. Phys.: Condens. Matter* **21** 164219 (2009).

18 R McFee, Optimum input leads for cryogenic apparatus, *Rev. Sci. Instrum.* **30** 98 (1959).

19 A Ballarino, Current leads for the LHC magnet system, *IEEE Trans. Appl. Supercond.* **12** 1275 (2002).

20 N Mitchell *et al*, The ITER magnet system, *IEEE Trans. Appl. Supercond.* **18** 435 (2008).

21 A Shajii and J P Freidberg, Quench in superconducting magnets. I. Model and numerical implementation, *J. Appl. Phys.* **76** 3149 (1994).

22 V D Arp and R D McCarty, *Thermophysical Properties of Helium-4 from 0.8 to 1500 K with Pressures to 2000 MPa*, NIST Technical Note 1334 (revised) (Boulder, CO: NIST, 1998).

23 R P Reed and A F Clark (eds), *Materials at Low Temperatures* (Metals Park, OH: American Society for Metals, 1983).

24 M Marchevsky, Quench detection and protection for high-temperature superconductor accelerator magnets, *Instruments* **5** 27 (2021). doi:10.3390/instruments5030027

25 E E Salazar *et al*, Fiber optic quench detection for large-scale HTS magnets demonstrated on VIPER cable during high-fidelity testing at the SULTAN facility, *Supercond. Sci. Technol.* **34** 035027 (2021). doi:10.1088/1361-6668/abdba8

26 R Teyber, J Weiss, M Marchevsky, S Prestemon and D van der Laan, Current distribution monitoring enables quench and damage detection in superconducting fusion magnets, *Sci. Rep.* **12** 22503 (2022). doi:10.1038/s41598-022-26592-2

27 J E Menard *et al*, Fusion nuclear science facilities and pilot plants based on the spherical tokamak, *Nucl. Fusion* **56** 106023 (2016).

COLOPHON

How this document was made

The Kronos Fleet — Combined Editorial, 2026 is set in **Fraunces** (display), **Gelasio** (text), and **IBM Plex Mono** (data & equations), carried forward from the Kronos editorial design system.

The figures are rendered at 300 dpi from the deposited generator scripts; the document is composed as a single self-contained file with embedded fonts and imagery, paginated to US Letter, and rendered to PDF through a headless Chromium engine in matched light and dark editions.

Every headline quantity carries an evidence class; withdrawn and restated values are marked as such. Nothing herein is frozen beyond the founder-approved Tier-A set.

Explore it live — turn the interactive 3-D model, run the deposited solvers in the physics validator, and watch the companion film series.

LEGAL NOTICE

Notice, status, and distribution

Conceptual design & simulation study. This document reports a conceptual design and simulation study. It is not a construction commitment, a safety-analysis report, a regulatory filing, or an offer of securities. Forward-looking statements — schedules, costs, market sizes, and performance — are estimates subject to the limitations set out in the Simulations part and may change.

Numbers and their classes. Quantities are reported with evidence classes and case labels; modelled, assumed, and requirement-class values are identified as such and are not to be quoted without their labels.

Public edition. This edition carries the physics and design only; all financial, funding, and defense-commercial content has been removed for public distribution. The scientific text corresponds to the arXiv and journal submissions.

THE 2026 KRONOS SERIES

One programme, many papers

This editorial is one paper in the Kronos 2026 series — a real fusion company's complete, reproducible physics record for a spherical-tokamak breeder and its low-neutron D–^{3}He tandem-mirror burners. Every headline number is a frozen anchor in the Physics De-Risking Register.

Explore the whole programme: the De-Risking Register, the interactive 3-D model, and the physics validator.

KRONOS FUSION ENERGY

Cryogenics and the Cold-Mass Thermal Budget of a High-Field Spherical-Tokamak Breeder: Centrepost Heat Loads, Current Leads, and the 4.5 K Refrigeration Plant

A real fusion company building real machines. Explore the science, live.

Zenodo · doi:10.5281/zenodo.22645840

Read on kronosfusionenergy.com

The Physics De-Risking Register